MDPI

Article

Genome-scale metabolic model of infection with SARS-CoV-2 mutants confirms guanylate kinase as robust potential antiviral target

Alina Renz [1,2,3], Lina Widerspick [4], and Andreas Dräger [1,2,3,5,*]

[1] Computational Systems Biology of Infections and Antimicrobial-Resistant Pathogens, Institute for Bioinformatics and Medical Informatics (IBMI), University of Tübingen, 72076 Tübingen, Germany
[2] Department of Computer Science, University of Tübingen, 72076 Tübingen, Germany
[3] Cluster of Excellence 'Controlling Microbes to Fight Infections,' University of Tübingen, 72076 Tübingen, Germany
[4] Bernhard Nocht Institute for Tropical Medicine, 20359 Hamburg, Germany
[5] German Center for Infection Research (DZIF), partner site Tübingen, 72076 Tübingen, Germany
* Correspondence: draeger@informatik.uni-tuebingen.de

Abstract: The current SARS-CoV-2 pandemic is still threatening humankind. Despite first successes in vaccine development and approval, no antiviral treatment is available for COVID-19 patients. The success is further tarnished by the emergence and spreading of mutation variants of SARS-CoV-2, for which some vaccines are not effective anymore. This highlights the urgent need for antiviral therapies even more. This article describes how the genome-scale metabolic model (GEM) of the host-virus interaction of human alveolar macrophages and SARS-CoV-2 was refined by incorporating the latest information about the virus's structural proteins and the mutant variants B.1.1.7 and B.1.351. We confirmed the initially identified guanylate kinase as a potential antiviral target with this refined model and identified further potential targets from the purine and pyrimidine metabolism. The model was further extended by incorporating the virus' lipid requirements. This opened new perspectives for potential antiviral targets in the altered lipid metabolism. Especially the phosphatidylcholine biosynthesis seems to play a pivotal role in viral replication. The guanylate kinase is even a robust target in all investigated mutation variants currently spreading worldwide. These new insights can guide laboratory experiments for the validation of identified potential antiviral targets. Only the combination of vaccines and antiviral therapies will effectively defeat this ongoing pandemic.

Keywords: SARS-CoV-2, COVID-19, flux balance analysis (FBA), genome-scale metabolic models, target identification, reaction knock-out, structural proteins, purine metabolism, pyrimidine metabolism, B.1.1.7, B.1.351

1. Introduction

Since its emergence in December 2019 [1], individual cases of Severe Acute Respiratory Syndrome (SARS)-CoV-2 infections have evolved into an uncontrolled pandemic. As a result, more than 2.8 million people have lost their lives to or with Coronavirus Disease 19 (COVID-19) by March 2021. COVID-19 symptoms range from pneumonia to severe lung, heart, liver, kidney, neurological or gastrointestinal dysfunction [2]. While great efforts have been employed to provide effective SARS-CoV-2 vaccines [3,4], their success is overshadowed by the emergence of viral escape mutants and the shortcomings in developing targeted antiviral treatments. A meta-analysis by Liu *et al.* demonstrates that in non-severe cases of COVID-19, there is little to no evidence for effective use of ribavirin, hydroxychloroquine, umifenovir, lopinavir/ritonavir, or interferon [5]. Even the putative effectiveness of remdesivir is questionable [6,7].

While antiviral medication development was less fruitful, as of March 2021, there are 13 vaccines for SARS-CoV-2 in use, most of them targeting the spike (S) protein [3,8]. Albeit the successes in vaccine development, reports of mutations are increasing. Some of these mutations are even bypassing the immunity provided by several vaccine candidates. Four mutation variants have prevailed, disseminate rapidly, and are classified as variants of concern: (i) B.1.1.7, first detected in the United Kingdom; (ii) P.1 (also called B.1.1.28), first detected in Japan and Brazil; (iii)B.1.351, first detected in South Africa; and (iv)B.1.427/B.1.429, first detected in the US [9,10]. While the consequences of some of these mutations for vaccine efficacy have been reported, the metabolic implications of them remain unclear.

SARS-CoV-2 is a member of the *Betacoronavirus* genus within the *Nidovirales* order [4,11]. The virus has a 27 to 32 kb positive sense, single-stranded RNA genome encoding 26 proteins, including the four structural proteins spike (S), envelope (E), matrix (M) and nucleoprotein (N) [4,12]. The S trimers [13,14] scan the host cells surface for the viral entry receptor angiotensin converting enzyme 2 (ACE-2) and therefore initiate the entry process [1,4]. The structural proteins E and M facilitate viral transport, assembly, budding, and release of SARS-CoV-2 virions from infected host cells [1,4]. While N is expressed within the host cytoplasm, the other structural proteins S, E, and M are translated within the endoplasmic reticulum–Golgi intermediate compartment (ERGIC) of the host cell [2,4]. SARS-Cov-2 N supports replicating the viral genome in the cytoplasm and encloses novel viral RNA to form viral ribonucleoprotein complexes (vRNPs) [2]. During the viral replication process's final steps, these cytoplasmic vRNPs are assembled with S, E, and M proteins within the ERGIC [2,4]. The mature virions bud at the ERGIC membrane, forming vesicles which are subsequently released from the host cell via exocytosis [2,4].

Viral lipid envelopes protect the vRNPs and facilitate the particles' entry into host cells [15]. They are usually acquired via budding from the plasma membrane or other cellular organelles [15,16]. Viruses specifically modify host membrane structures, the composition, and the whole host lipid metabolism to favor viral replication [15,17,18]. Many viruses exploit spatiotemporally enriched microdomains or rafts containing different lipid species [18]. To this end, cholesterol, for instance, increases host membrane fluidity for efficient viral entry, replication, and budding, while phosphatidylserine supports viral entry [18]. Altogether, various modifications in viral egress areas determine the differing composition of viral envelopes, thereby influencing their stability and infectivity [18]. As SARS-CoV-2 buds from the ERGIC [2,4], its envelope lipid bilayer resembles this host organelle's composition [2,4]. The viral membrane formation mostly requires cholesterol and phospholipids, while sphingomyelin and cardiolipin are presumably less abundant [19,20].

In our previous work, we have generated an integrated human-virus metabolic model, which combines flux balance analysis (FBA) and flux variability analysis (FVA) to model the metabolic changes within SARS-CoV-2 infected human alveolar macrophages [21]. The GEM is based on the already published and well-developed human alveolar macrophage model iAB-AMØ-1410 by Bordbar *et al.* [22] and was employed to predict putative antiviral targets such as guanylate kinase 1 (GK1) or the availability of L-isoleucine and L-lysine [21]. Some of these potential targets may be directly targeted by small molecules or antivirals [23–25]. Increasing knowledge of SARS-CoV-2 facilitates the model's improvement by incorporating recent findings of the copy number of the structural proteins [21,26]. The stoichiometric coefficients of the metabolic requirements for amino acids and nucleotides and energy requirements can be refined to predict the viral replication capacity better. Additionally, the lipid requirements were now accounted for in the viral biomass objective function (VBOF). This study presents an updated version of the integrated alveolar macrophage SARS-CoV-2 GEM and the consequences of prominent mutations for predicted metabolic targets.

Preprints (www.preprints.org) | NOT PEER-REVIEWED | Posted: 30 April 2021 doi:10.20944/preprints202104.0788.v1

Table 1: Copy number of structural proteins. The copy number of structural proteins (Csp) was determined based on extensive literature research. Besides the reference and the copy number of structural proteins, the investigated organism is given as a source.

Protein	Name	Reference	Source	Csp
S	spike	Turoňová *et al.*	SASRS-CoV-2	120
E	envelope	Tilocca *et al.*	hCOV, TGEV	20
N	nucleocapsid	Klein *et al.*, Yao *et al.*	SARS-CoV-2	456
M	membrane	Neuman *et al.*	SARS-CoV-1	1000

2. Results

2.1. Correcting the copy number of structural proteins

The single-stranded RNA genome of SARS-CoV-2 has 26 proteins [12], including four structural proteins. These four structural proteins need to be produced by the host in higher amounts than the non-structural proteins. However, the actual number of copies of each structural protein was unknown when the novel coronavirus arose, and the first studies were conducted at the beginning of the year 2020.

After extensive literature research, we collected the latest information about the copy number of the structural proteins of SARS-CoV-2. Turoňová *et al.* identify on average 40 copies of the trimeric spike (S) protein on the surface of SARS-CoV-2, resulting in 120 copies of the S protein. Klein *et al.* estimate the number of S trimers per virion to be 48, resulting in a similar copy number range as Turoňová *et al.* Since [14] used *in situ* structural analysis and Klein *et al.* use mathematical estimations, we chose to use a copy number of 120 S proteins for further analysis (see table 1). The number of the envelope (E) proteins is approximated to 20 copies [27] based on analyses of the OC43 human coronavirus (hCOV) [28] and the transmissible gastroenteritis virus (TGEV) [29]. The nucleocapsid (N) packs the viral RNA in so-called vRNPs. Klein *et al.* observe 38 vRNPs per SARS-CoV-2 virion [13]. Approximately 12 copies of the N protein are located in one vRNP in SARS-CoV-2 [30,31]. Multiplying those two numbers results in 456 copies of the N protein. The amount of membrane (M) proteins is not yet determined for SARS-CoV-2. Bar-On *et al.* provide key numbers about SARS-CoV-2, including the copy numbers of the S, M, N, and E protein. However, all copy numbers are derived from SARS-CoV-1 or TGEV. We found precise numbers for the copy number of N proteins in SARS-CoV-2, and Neuman *et al.* determine the estimated ratios of M to N proteins ranging from 3M:1N to 1M:1N with 730 to 2200 N proteins per virion [32]. With this information at hand, we estimated the copy number of M proteins to 1000 by doubling the number of N proteins and rounding them up. The ratio of 2M:1n was chosen based on the article of Bar-On *et al.*, where the number of N proteins is stated as 1000 copies for SARS-CoV-1 and the number of M proteins as 2000. All used copy numbers are listed in table 1.

With the updated copy numbers, the stoichiometric coefficients of the nucleotides, amino acids, and energy requirements were re-calculated for the viral biomass objective function (VBOF) of SARS-CoV-2. The subsequent analyses for identifying potential antiviral targets consisted of knock-out and host-derived enforcement experiments, as Renz *et al.* describe [21]. The guanylate kinase (GK1) remains a promising antiviral target after the adaptions of the copy number of structural proteins based on the knock-out experiments.

The results of the host-derived enforcement analyses were dependent on the copy number of structural proteins [21]. As we know identified more precise copy numbers, we can also determine the host-derived enforcement analysis results more precisely. In total, 21 reactions were identified, whose inhibition decreases the viral replication capacity by at least 20 % without harming the host's maintenance (100 %). These reactions, their inhibition range, and the reduction of the VBOF are visualized in figure 1 on the following page. Reactions could be inhibited between 72 % and 89 %. As seen

Preprints (www.preprints.org) | NOT PEER-REVIEWED | Posted: 30 April 2021 doi:10.20944/preprints202104.0788.v1

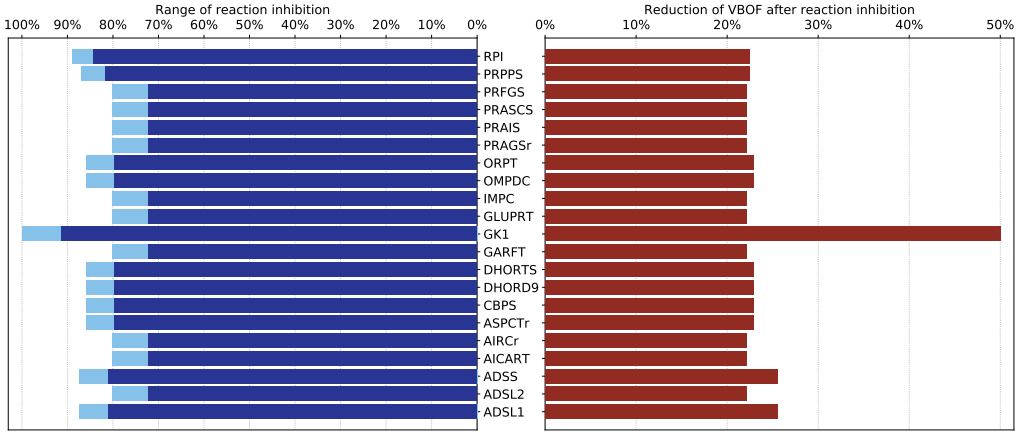

Figure 1. Results of the host-derived enforcement experiments. With the help of the host-derived enforcement, the range and effect of reaction inhibitions on the VBOF can be investigated while keeping the host's maintenance at 100 %. The minimum possible reaction inhibition rate to reduce the viral replication capacity (VBOF) is given in dark blue. The maximum inhibition of the reaction does not harm the host's maintenance and is indicated in light blue. The reduction of the VBOF is given in comparison to the un-inhibited state. All reaction identifiers are BiGG identifiers [35]. Table A1 lists all reaction identifiers with their corresponding reaction name and the subsystem they occur in.

in the knock-out experiments, the guanylate kinase (GK1) is the only reaction where a complete inhibition (100 %) is possible.

The ribose-5-phosphate isomerase (RPI) and phosphoribosylpyrophosphate synthetase (PRPPS) are part of the pentose phosphate pathway. Glutamine phosphoribosyldiphosphate amidotransferase (GLUPRT), phosphoribosylglycinamide synthase (PRAGSr), phosphoribosylglycinamide formyltransferase (GARFT) phosphoribosylformylglycinamidine synthase (PRFGS), phosphoribosylaminoimidazole synthase (PRAIS), Phosphoribosylaminoimidazole carboxylase (AIRCr), phosphoribosylaminoimidazolesuccinocarboxamide synthase (PRASCS), phosphoribosylaminoimidazolecarboxamide formyltransferase (AICART), and IMPC cyclohydrolase (IMPC) are involved in the purines' biosynthetic pathway, more precisely in the biosynthesis of inosine monophosphate (IMP) [33]. Reactions associated with the purine adenosine monophospate (AMP) biosynthesis were also identified as potential targets, namely adenylosuccinate synthase (ADSS), and adenylosuccinate lyase 1 and 2 (ADSL1, ADSL2) [33].

Besides the reactions associated with the purine metabolism, the host-derived enforcement analysis also reported reactions from the pyrimidine biosynthesis, such as the carbamoyl-phosphate synthase (CBPS), aspartate carbamoyltransferase (ASPCTr), dihydroorotase (DORTS), dihydoorotic acid dehydrogenase (DHORD9), orotate phosphoribosyltransferase (ORPT), and orotidine-5'-phosphate decarboxylase (OMPDC) [34].

2.2. Testing the targets' robustness for several mutations

Analysis of mutant-specific variations in the viral biomass

Novel mutations of SARS-CoV-2 emerge on a daily basis. Four mutation variants have prevailed, disseminate rapidly, and are classified as variants of concern: (i) B.1.1.7, (ii) P.1 (also called B.1.1.28), (iii) B.1.351, and (iv) B.1.427/B.1.429 [9,10]. The Global Initiative on Sharing All Influenza Data (GISAID) was launched in 2008 to promote the international sharing of virus data [36,37]. When the novel coronavirus emerged, GISAID was expanded by a database for sharing sequenced viral genomes of SARS-CoV-2 globally. At the time of writing, more than 850,000 viral sequences of SARS-CoV-2 are collected in the database. To investigate the mutations' effect on the previously identified

Preprints (www.preprints.org) | NOT PEER-REVIEWED | Posted: 30 April 2021 doi:10.20944/preprints202104.0788.v1

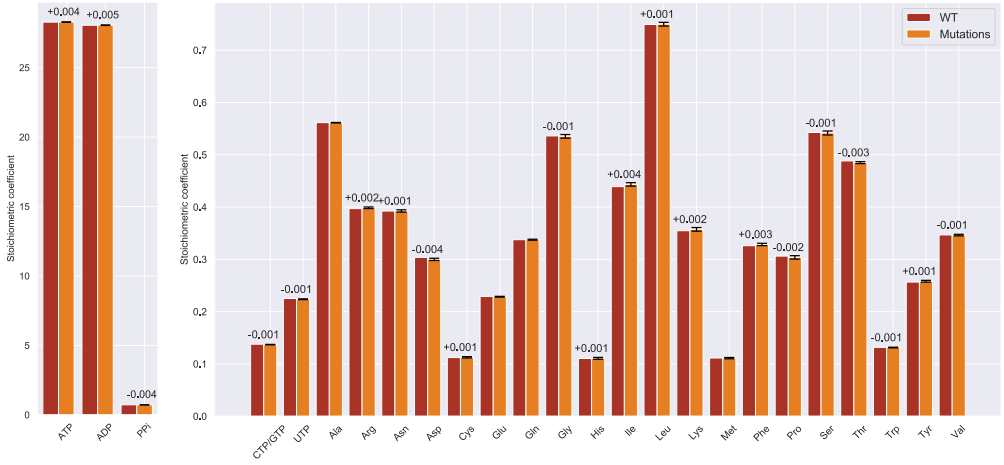

Figure 2. Difference of stoichiometric coefficients between wildtype (WT) and all mutations. The stoichiometric coefficients for all metabolites participating in the viral biomass objective function (VBOF) are compared. WT stoichiometric coefficients are indicated in red, the mean stoichiometric coefficients of all mutation variants are indicated in orange, including standard deviations (black). If the difference of the stoichiometric coefficients between WT and mutation variants was more than 0.001, the difference is indicated above the bars. The stoichiometric coefficients for the metabolites ATP, ADP and diphosphate (PPi), are higher compared to the other coefficients. The mutation variants' mean coefficients show little deviation. Additionally, the differences between the stoichiometric coefficients of WT and mutation variants are very small.

potential antiviral targets, sequences of each mutation variant were downloaded from GISAID and analyzed. The stoichiometric coefficients of each variant were calculated as Renz *et al.* describe [21]: For the calculation of the nucleotides' stoichiometric coefficients, the downloaded RNA sequence was used. The amino acids' stoichiometric coefficients were calculated using the provided information about the identified mutations and the reference (wildtype) protein sequence of the first sequenced SARS-CoV-2. With this information, the abundance of the different amino acids in the different proteins was adapted for each mutation variant. The nucleotide and amino acid counts were subsequently used to calculate the pyrophosphate liberation and the adenosine triphosphates (ATPs) requirements. For each downloaded mutation variant, an individualized VBOF was created with the calculated stoichiometric coefficients.

To assess the mutations' effect on the VBOF's stoichiometric coefficients, we first calculated the mean and standard deviation from all stoichiometric coefficients for all mutations and compared them to the wildtype (WT) coefficients. The mean stoichiometric coefficients of the mutations are very similar to the wildtpye's stoichiometric coefficents. The largest difference is observed for the two amino acids L-aspartate and L-isoleucine: The stoichiometric coefficient for L-aspartate is decreased by on average 0.004 in the mutations compared to the wildtype. In contrast, the stoichiometric coefficient for L-isoleucine is increased by on average 0.004 in the mutations. Figure 2 visualizes the comparison of the mutations' mean stoichiometric coefficients with the wildtype coefficients.

Since we analyzed four distinct mutation variants, the differences in the stoichiometric coefficients were examined further based on these variants. The mean for each stoichiometric coefficient was calculated variant-wise. With this mean, the deviation from the wildtype coefficient was calculated and visualized as a heat-map in figure 3 on the following page. This analysis gives further insight into the properties of the individual mutations.

One can observe a pattern for the stoichiometric coefficients of ADP and ATP: While the mutation variants B.1.1.7 and B.1.1.28 have decreased stoichiometric coefficients

Preprints (www.preprints.org) | NOT PEER-REVIEWED | Posted: 30 April 2021 doi:10.20944/preprints202104.0788.v1

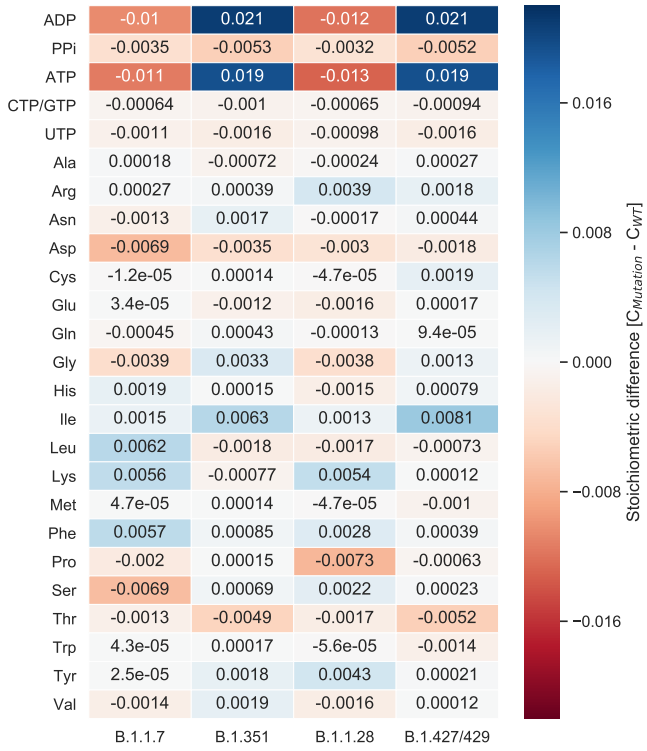

Figure 3. Difference of stoichiometric coefficients between wildtype (WT) and the individual mutations. The deviation between WT and the mean of the individual mutation variants was calculated. Higher stoichiometric coefficients in the mutation compared to the WT are indicated in blue, while lower stoichiometric coefficients are indicated in red. Based on similar sequence length for the mutation variants B.1.1.7 and B.1.1.28 and resulting similar total viral molar masses, a pattern emerges, which is most apparent for the stoichiometric coefficients of ATP and ADP. This pattern, however, is not present for all stoichiometric coefficients. The coefficient for L-serine, for example, is only decreased in the mutation variant B.1.1.7 based on two mutations in two structural proteins. Overall, the deviations from the WT are very small.

(−0.01) compared to the wildtype, the variants B.1.351 and B.1.427/429 have increased stoichiometric coefficients (0.019 to 0.021). This pattern is most apparent for adenosine diphosphate (ADP) and ATP, but can also be observed for other stoichiometric coefficients, such as for PPi, L-lysine, L-threonine, or -valine. To further investigate this pattern, we examined the calculation for the stoichiometric coefficients. Each coefficient is set in relation to the total viral molar mass (Mv), which is the sum of the total molar mass of all nucleotides (Gi) and amino acids (Gj). The mutation variants B.1.1.7 and B.1.1.28 have a higher total viral molar mass compared to the mutation variants B.1.351 and B.1.427/429. This increased total viral molar mass is based on an increased molar mass of both nucleotides (Gi) and amino acids (Gj). As the stoichiometric coefficients for ADP and ATP larger than the other coefficients, this pattern is more apparent.

However, this pattern does not emerge in all stoichiometric coefficients. There are deviations for, e.g., L-serine. Only the mutation variant B.1.1.7 shows a decreased stoichiometric coefficient compared to the wildtype. We analyzed the documented mutations for this variant and identified two mutations in structural proteins, `Spike S982A` and `N S235F`, which only occur in this variant. In both cases, the amino acid L-serine is substituted by another amino acid. As both mutations occur in structural proteins with copy numbers of 120 and 456, respectively, their influence on the amount of amino acid and, thus, the stoichiometric coefficient, is noticeable. Compared to the other mutation variants, variant B.1.1.28 has the highest increase in the stoichiometric

Preprints (www.preprints.org) | NOT PEER-REVIEWED | Posted: 30 April 2021 doi:10.20944/preprints202104.0788.v1

coefficient for L-serine. This could be explained by two mutations specific for this variant in the structural spike protein: `Spike P26S` and `Spike R190S`. In both cases, other amino acids are replaced by `l`-serine. As explained for the mutation variant B.1.1.7, the spike protein has a copy number of 120. Changes in these structural proteins can be measurable and influence the stoichiometric coefficient stronger than mutations in non-structural proteins.

Analysis of the effects of single gene deletions

After highlighting the differences in the stoichiometric coefficients for the different mutation variants, we tested the robustness of our previously identified potential antiviral targets [21]. To do so, we repeated the single-gene-deletion experiments for every mutation variant. Our analysis revealed that in all mutation variants, the guanylate kinase (GK1) is a robust potential antiviral target.

2.3. Lipids as part of the viral biomass objective function

The transmembrane domain of the envelope (E) protein is located in lipid bilayers mimicking the endoplasmic reticulum–Golgi intermediate compartment (ERGIC) membrane [20]. Schweizer *et al.* describe this ERGIC membrane [19] in 1994. The four phospholipids, phosphatidylcholine, phosphatidylethanolamine, phosphatidylinositol, and phosphatidylserine, were observed in the ERGIC while sphingomyelin and cardiolipin were not present [19]. Mandala *et al.* use an ERGIC-mimetic consisting of the four described phospholipids and cholesterol to investigate the E-protein's transmembrane domain [20]. The five lipids are also participating in the macrophage's maintenance function. Thus, their role and influence on the VBOF and antiviral targets were examined.

As the actual amount of lipids in the SARS-CoV-2 virion is not yet determined, we evaluated varying stoichiometric coefficients. In the first experiments, the individual lipids' effect on the VBOF's objective value was analyzed. The objective coefficients from the macrophage's maintenance function varied between 0.001 for phosphatidylserine and 0.031 for phosphatidylcholine. Therefore, we first varied all lipids' coefficients between 0 and 0.5 and subsequently used a multiplication coefficient between 0 and 10 to multiply the macrophage's coefficients. Despite an up to 490-fold increase of the stoichiometric coefficient (for phosphatidylserine) compared to its initial value in the macrophage's maintenance function, the VBOF's objective value remained at $0.01886\,\mathrm{mmol}/(\mathrm{gDW}\cdot\mathrm{h})$. This was also the case when all five lipids were added to the VBOF simultaneously.

Knock-out experiments were conducted to identify additional potential antiviral targets. All lipids were included in the VBOF, and the coefficients were varied using a multiplication coefficient. At the five-fold increase of the initial stoichiometric coefficients, two novel reactions emerged as new potential antiviral targets: the methionine synthase (`METS`) and the 5,10-methylenetetrahydrofolate reductase (FADH2) (`MTHFR`). To identify, which lipids are responsible for the emergence of the novel antiviral target, we repeated the described analysis for every lipid individually, once using absolute stoichiometric coefficients ranging from 0 to 0.5 and once using the above-described multiplication coefficient ranging between 0 and 10. By this approach, we identified phosphatidylcholine to be the responsible lipid for the additional antiviral targets. When increasing the initial macrophage's stoichiometric coefficient of phosphatidylcholine by at least 4.76, the two enzymes emerge as potential antiviral targets. At a five-fold increase of phosphatidylcholine and the knock-out of either the methionine synthase or the 5,10-methylenetetrahydrofolate reductase (FADH2), the viral growth can be inhibited by approximately 1.5 %. With increasing amounts of phosphatidylcholine in the VBOF, the knock-out influence of the two reactions on the viral growth increases, as seen in figure 4 on the next page: at an eleven-fold increase of phosphatidylcholine, the viral growth rate is decreased by approximately 50 %. A twenty-fold increase of phosphatidylcholine inhibits the viral growth even to 30 % of its initial growth rate.

Preprints (www.preprints.org) | NOT PEER-REVIEWED | Posted: 30 April 2021 doi:10.20944/preprints202104.0788.v1

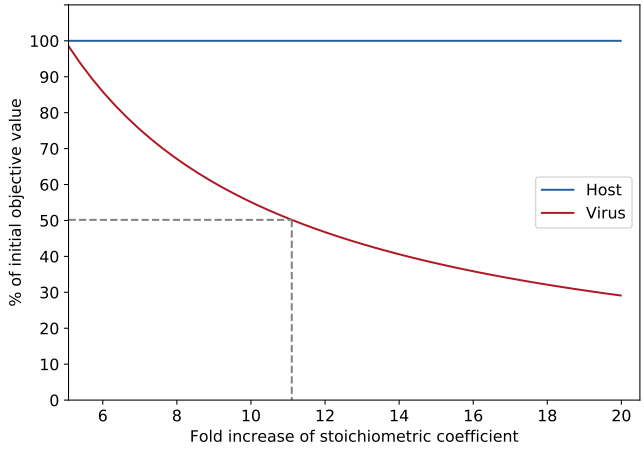

Figure 4. Influence of stoichiometric coefficient on reduction of VBOF during METS knock-out. With increasing factorization of phosphatidylcholine's stoichiometric coefficient, the objective value of the VBOF's optimization decreases during the knock-out of the methionine synthase (METS) reaction. The hosts growth maintenance stays at 100 %. At an eleven-fold increase of the initial stoichiometric coefficient extracted from the host's maintenance function results in a 50 % decrease of the viral growth rate.

It needs to be highlighted that the guanylate kinase (GK1) was a potential antiviral target during all conducted *in silico* experiments evaluating the lipids' effect on potential targets.

3. Discussion

This study presents an updated viral biomass objective function (VBOF) for the novel coronavirus SARS-CoV-2 based on the latest information of its structural proteins. This VBOF was integrated into an already validated model of human alveolar macrophages [22].

The tissue tropism of SARS-CoV-2 comprises most cell types expressing the entry receptor ACE-2, mainly including cell types of the lung, liver, stomach, ileum, kidney, and colon [38,39]. Although SARS-CoV-2 enters the host via the airways, the expression of ACE-2 is comparably low, highlighting the role of possible co-receptors [39]. Nonetheless, human alveolar type 2 cells robustly express ACE-2, while alveolar macrophages possibly express low levels of the entry receptor [39]. It is known that different coronaviruses infect macrophages, such as the human coronavirus strain 229E [40], the Middle East Respiratory Syndrome (MERS) coronavirus [41], and the SARS coronavirus [42]. Also, the novel coronavirus SARS-CoV-2 is reported to infect alveolar macrophages [43]. However, other *in vitro* studies suggest that challenging alveolar macrophages with SARS-CoV-2 does not lead to a productive infection [44]. However, even without productive infection, alveolar macrophages could serve as Trojan horses, which enable viral anchoring within pulmonary parenchyma [38]. Dalskov *et al.* demonstrate that the tissue-resident alveolar macrophages play a crucial role in SARS-CoV-2 immune evasion [43,44] and are hypothesized to support viral pathogenesis [38]. Disabling viral replication in human alveolar macrophages might be an early way of intervention and prevention of the virus's further spread.

We corrected the copy number of structural proteins and the stoichiometric coefficients in the viral biomass objective function (VBOF). The amount of the spike (S) and nucleocapsid (N) proteins were derived from studies on SARS-CoV-2 [13,14,30]. The copy number of the envelope (E) protein is derived from the human coronavirus and the transmissible gastroenteritis virus [27]. Numbers for SARS-CoV-2 are currently not available. Same accounts for the copy number of membrane (M) proteins, where information is only available for SARS-CoV-1 [32]. Especially for the M proteins, a range

of potential copy numbers exists, as the ratio of M and N proteins ranges from 3M:1N to 1M:1N [32]. With the N protein's copy number of 456, the M protein's copy number ranges from 456 to 1368. As soon as additional information on the copy numbers of the E and M protein is available for SARS-CoV-2, the stoichiometric coefficients can be refined further.

However, the current refinement still confirmed the guanylate kinase (GK1) as a potential antiviral target. Even for the investigated mutations, the guanylate kinase seems to be a robust target in human alveolar macrophages to interrupt SARS-CoV-2 replication. Delattre *et al.* conduct a similar study with the human reconstruction RECON2.2 [46] containing a lung biomass objective function and a viral biomass objective function [45]. They also report the guanylate kinase as a potential target for antiviral therapies [45]. In our previous study, we suggested potential drugs that could be repurposed to fight this SARS-CoV-2 pandemic. Amongst these drugs were cidofovir, brincidofovir, and favipiravir [21]. A virtual screening method identified cidofovir as a potentially effective therapeutic against SARS-CoV-2 [47]. A molecular docking study suggests the repurposing of brincidofovir against SARS-CoV-2 [48]. For favipiravir, several clinical trials are listed in the ClinicalTrials database hosted by the U.S. National Library of Medicine [49], running in several countries, including Italy (NCT04336904), Turkey (NCT04474457), and the United States (NCT04358549). However, these therapeutics are only analogs and do not directly inhibit the guanylate kinase. No direct inhibitor of the guanylate kinase is tested for its antiviral effect on SARS-CoV-2 infections at the time of writing. As the guanylate kinase is a robust target for all currently occurring mutation variants, further investigations could be of high interest to fight this pandemic.

Besides the guanylate kinase, additional potential antiviral targets were identified using the host-derived enforcement analysis. These antiviral targets are located in the pentose phosphate pathway, the purine, and the pyrimidine metabolism. It is shown that the pentose phosphate pathway is remarkably deregulated during SARS-CoV-2 replication, which shows potential implications for antiviral therapies [50]. The purine biosynthesis pathway is enhanced upon SARS-CoV-2 infection to support the *de novo* synthesis of purines [51]. First *in vitro* experiments show that the FDA-approved inhibitor of purine biosynthesis methotrexate potently inhibits viral replication [52,53], protein synthesis, and release [52]. The pyrimidine metabolism is also reported as a potential antiviral target, especially the dihydroorotate dehydrogenase. Its inhibition by, for example, brequinar or leflunomide is already demonstrated to have antiviral activity against other viruses [54–56], such as rotavirus [57] and Ebola virus [58]. The dihydroorotate dehydrogenase inhibitor PTC299 is shown to arrest SARS-CoV-2 replication *in vitro* [59]. The dihydroorotate dehydrogenase inhibitors S312 and S416 are validated to have high antiviral efficacy *in vivo* [60]. To conclude, our identified antiviral targets are currently under discussion in the scientific community, and for some, the influence and relevance for viral replication are confirmed.

Alongside the mutation variants that could complicate the fight against SARS-CoV-2 with vaccines, the S protein's glycosylation could impact antibodies' ability to bind to a pathogenic S glycoprotein by shielding its surface [61,62]. Currently, this glycosylation process is not reflected in the VBOF or the model. As soon as more information about the glycosylation is available that can be used to determine a range or precise stoichiometric coefficients, the glycosylation of the spike protein can be incorporated into the model simulations.

The inclusion of lipids in the VBOF opens new perspectives for potential antiviral targets. It is shown that virus infections can dramatically impact on lipid metabolism [63–66]. Upon rhinovirus infection multiple lipid pathways are altered, and changes in phospholipids, lysophospholipids, fatty acids, and inositol phospholipids are observed [65]. For the human coronavirus 229E (hCoV-229E), the host cell lipid response upon infection was comprehensively characterized. Glycerophospholipids and fatty acids were significantly elevated. Lysophosphatidylcholine, which is hydrolyzed from phos-

phatidylcholine, was significantly elevated and accounted for approximately 60 % of all identified lipids with significant elevation [67]. Our study also highlighted phosphatidylcholine as an essential lipid upon SARS-CoV-2 infection, confirming the findings from Yan *et al.* for hCoV-229E. As metabolic alterations harbor potential antiviral targets, regulating or targeting the lipid metabolism is suggested and discussed [63,65,67]. We identified two novel potential antiviral targets connected with lipid metabolism: the methionine synthase and the 5,10 methylenetetrahydrofolate reductase. S-adenosyl-L-methionine is a pivotal methyl donor in the synthesis of phosphatidylcholine [68,69]. Thus, the synthesis of L-methionine by the 5-10 methylenetetrahydrofolate reductase and methionine synthase seem to be an antiviral target to disrupt the synthesis of phosphatidylcholine. These novel insights could guide further laboratory experiments for investigating and validating the lipid's role in SARS-CoV-2 infections.

This study confirmed the guanylate kinase GK1 as a robust antiviral target against SARS-CoV-2 and its arising mutation variants. With the refined copy numbers of structural proteins, the list of further potential antiviral targets was improved, and some targets are already under discussion or even under validation. The inclusion of the lipids into the VBOF opened new perspectives for additional metabolic targets to fight against this pandemic.

4. Materials and Methods

4.1. Correcting the copy number of structural proteins

In the previous version of the VBOF, the copy number of structural proteins was not yet known. We conducted extensive literature research to identify the precise copy number of each structural protein individually. The search was mainly focused on SARS-CoV-2 directly. However, if no information was found for the novel coronavirus, we also searched for information on closely related coronaviruses.

With the identified copy numbers (see table 1 on page 3), the stoichiometric coefficients of the nucleotides, amino acids, and energy requirements were re-calculated, as Renz *et al.* state [21]. However, instead of using a general copy number for all structural proteins, as Aller *et al.* describe [26], the individual copy numbers of the respective structural proteins were used.

After the VBOF was updated with the corrected stoichiometric coefficients, the knock-out and host-derived enforcement analyses were repeated, as Renz *et al.* describe [21]. The knock-out experiments were performed by subsequently knocking out each reaction and evaluating its effect on the host's maintenance and viral replication capacity (VBOF). For the host-derived enforcement analyses, the FVA was used to determine flux ranges that allow for 100 % maintenance of the host, while decreasing the viral growth by at least 20 %. The adapted host-derived enforcement algorithm was used, as Renz *et al.* describe [21].

4.2. Testing the targets' robustness against for several mutations

The Global Initiative on Sharing All Influenza Data (GISAID) database has a collection of more than 850,000 viral sequences of SARS-CoV-2 (March 2021). We set the following filters for the sequences: (i) variant (VUI202012/01 GRY (B.1.1.7) for variant B.1.1.7; GH/501Y.v2 (B.1.351) for variant B.1.351; GR/501Y.V3 (P.1) for variant B.1.1.28; and GH/452R.V1 (B.1.429+B.1.427) for variants B.1.429 and B.1.427) and (ii) location (Europe/United Kingdom for variant B.1.1.7; Africa for variant B.1.351; South America for variant B.1.1.28; and North America/USA for variants B.1.429 and B.1.427. We randomly downloaded ten sequences from each mutation variant with the filters set as described. In addition to the sequences, we downloaded the mutation information given in the metadata. With this information, the stoichiometric coefficients for the VBOF were calculated for every downloaded mutation. As the calculation of the nulceotides' stoichiometric coefficients requires the nulceotide sequence, the downloaded sequences were used directly for this step. For the calculation of the amino acids' coefficients,

Preprints (www.preprints.org) | NOT PEER-REVIEWED | Posted: 30 April 2021 doi:10.20944/preprints202104.0788.v1

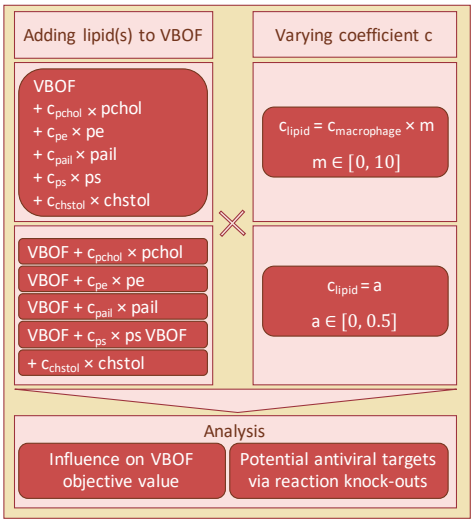

Figure 5. Workflow for the investigation of lipids' influence on the VBOF. The five lipids phosphatidylcholine (pchol), phosphatidylethanolamine (pe), phosphatidylinositol (pail), phosphatidylserine (ps), and cholesterol (chstol) were added together and individually to the VBOF. The stoichiometric coefficients were either an absolute value identical for all lipids, or the initial stoichiometric coefficient from the macrophage biomass function factorized with a multiplication-coefficient. For all scenarios, the influence of the different VBOFs on the objective value was analyzed. Additionally, potential antiviral targets were examined using reaction knock-outs.

we used the annotated protein sequence of the SARS-CoV-2 reference sequence (NCBI accession: `NC_045512.2`) and the mutation information extracted from the metadata files. An algorithm adapted the amino acids from the protein sequence in accordance with the defined mutations, including substitutions, deletions, and introductions of stop codons. With the calculation of the energy requirements and pyrophosphate liberation, all stoichiometric coefficients for the VBOF were available and could be compared. For the first comparison, the mean and standard deviation of all mutations was calculated for each coefficient. These mean values were compared to the wildtpye (WT) stoichiometric coefficients by calculation the difference. In subsequent analysis, the mean was calculated for the four mutation variants and was then compared to the wildtype. Again, the difference between the coefficients was calculated and visualized. With all generated VBOFs, the reaction knock-out experiments were repeated, as described in the previous section.

4.3. Lipids as part of the viral biomass objective function

Literature research was conducted to identify potential fatty acids that occur in the capsid of SARS-CoV-2. As no lipidomics data of SARS-CoV-2 existed at the time of writing, we focused on the five identified lipids phosphatidylcholine, phosphatidylethanolamine, phosphatidylinositol, phosphatidylserine, and cholesterol. The influence of the individual lipids' inclusion into the VBOF on the objective value when optimizing for the VBOF was evaluated. An overview of the overall procedure for testing the lipids' influence is given in figure 5.

As no data were available for the amount of the respective lipids in one virion, we varied the stoichiometric coefficients between 0 and 0.5. The stoichiometric coefficients of the lipids within the macrophage's biomass maintenance function varied from 0.00102 for phosphatidylserine to 0.0315 for phosphatidylcholine (see also table 2 on the following page).

With the variation of the stoichiometric coefficients between 0 and 0.5, we covered the 14- to 490-fold increase of the stoichiometric coefficients, depending on their initial value. In the next step, all lipids were added simultaneously to the VBOF. We evaluated the VBOF's objective value using both the lipids' stoichiometric coefficients from the macrophage's maintenance function and their ten-fold value.

To evaluate the effect of the lipids' inclusion on the potential antiviral targets, we again used the stoichiometric coefficients of the macrophage's maintenance function and a multiplication coefficient, ranging from 0 to 10 as the actual coefficient of the lipids is unknown. We conducted the knock-out experiments as Renz *et al.* describe [21] for each tested coefficient by knocking out each reaction individually and analyzing its

Table 2: Stoichiometric coefficients of the five lipids in the macrophage's maintenance function. The stoichiometric coefficients of the five lipids were extracted from the macrophage's maintenance function. Additionally, the BiGG identifiers [35] of the lipids are given. These stoichiometric coefficients formed the starting point for evaluating the lipids' influence on the viral biomass objective function (VBOF).

Lipid	BiGG ID	Coefficient
Phosphatidylcholine	`pchol_hs_c`	0.03152
Phosphatidylethanolamine	`pe_hs_c`	0.02110
Phosphatidylinositol	`pail_hs_c`	0.00374
Phosphatidylserine	`ps_hs_c`	0.00102
Cholesterol	`chsterol_c`	0.02093

effect on both the viral growth and the host's maintenance function. While varying the multiplication coefficient, two additional reactions occurred, whose knock-out decreased the viral growth rate.

To investigate, which lipid influences the knock-out experiments most, we again analyzed the lipids individually. As done for the effect on the VBOF's objective value, we first varied the stoichiometric coefficients between 0 and 0.5. Subsequently, we used a multiplication coefficient ranging from 0 to 10, which was multiplied with the coefficient of the macrophage's maintenance function (see table 2).

Author Contributions: Conceptualization, A.R. and A.D.; methodology, A.R. and L.W.; investigation, A.R. and L.W.; software, A.R.; visualization, A.R.; supervision, A.D.; funding acquisition, A.D.; writing—original draft preparation, A.R. and L.W.; writing—review and editing, A.R., L.W., and A.D; All authors have read and agreed to the published version of the manuscript.

Funding: This work was funded by the Federal Ministry of Education and Research (BMBF) and the Baden-Württemberg Ministry of Science as part of the Excellence Strategy of the German Federal and State Governments, by the *Deutsche Forschungsgemeinschaft* (DFG, German Research Foundation) under Germany's Excellence Strategy – EXC 2124 – 390838134, and supported by the German Center for Infection Research (DZIF, doi: 10.13039/100009139) within the *Deutsche Zentren der Gesundheitsforschung* (BMBF-DZG, German Centers for Health Research of the Federal Ministry of Education and Research), grant № 8020708703. The authors acknowledge support by the Open Access Publishing Fund of the University of Tübingen (https://uni-tuebingen.de/de/58988).

Data Availability Statement: The genome-scale metabolic model of the human alveolar macrophage infected with SARS-CoV-2 is available in the BioModels Database [70] as an SBML Level 3 Version 1 file [71–73] with the flux balance constraints (fbc) extension package [74] within a COMBINE Archive OMEX file [75] under the accession number `MODEL2003020001`.

Conflicts of Interest: The authors declare no conflict of interest.

Abbreviations

The following abbreviations are used in this manuscript:

ACE-2	angiotensin converting enzyme 2
ADP	Adenosine diphosphate
ATP	Adenosine triphosphate
COMBINE	Computational Modeling in Biology Network
COVID-19	Coronavirus Disease 2019
E	envelope
ERGIC	endoplasmic reticulum-Golgi intermediate compartment
FBA	flux balance analysis
fbc	flux balance constraints
FVA	flux variability analysis
GEM	genome-scale metabolic model
GISAID	Global Initiative on Sharing All Influenza Data
GK1	Guanylate kinase 1
hCOV	human coronavirus
hCoV-229E	human coronavirus 229E
M	Matrix
MERS	Middle East Respiratory Syndrome
N	nucleoprotein
OMEX	Open Modeling Exchange format
S	spike
SARS	Seere Acute Respiratory Syndrome
SBML	Systems Biology Markup Language
TGEV	transmissible gastroenteritis virus
VBOF	viral biomass objective function
vRNP	viral ribonucleoprotein complex

References

1. Zhou, P.; Yang, X.L.; Wang, X.G.; Hu, B.; Zhang, L.; Zhang, W.; Si, H.R.; Zhu, Y.; Li, B.; Huang, C.L.; Chen, H.D.; Chen, J.; Luo, Y.; Guo, H.; Jiang, R.D.; Liu, M.Q.; Chen, Y.; Shen, X.R.; Wang, X.; Zheng, X.S.; Zhao, K.; Chen, Q.J.; Deng, F.; Liu, L.L.; Yan, B.; Zhan, F.X.; Wang, Y.Y.; Xiao, G.F.; Shi, Z.L. A pneumonia outbreak associated with a new coronavirus of probable bat origin. *Nature* **2020**, *579*, 270–273. doi:10.1038/s41586-020-2012-7.
2. Mirtaleb, M.S.; Mirtaleb, A.H.; Nosrati, H.; Heshmatnia, J.; Falak, R.; Zolfaghari Emameh, R. Potential therapeutic agents to COVID-19: An update review on antiviral therapy, immunotherapy, and cell therapy. *Biomedicine & Pharmacotherapy* **2021**, *138*, 111518. doi:10.1016/j.biopha.2021.111518.
3. Li, D.D.; Li, Q.H. SARS-CoV-2: vaccines in the pandemic era. *Military Medical Research* **2021**, *8*, 1. doi:10.1186/s40779-020-00296-y.
4. Zhao, J.; Zhao, S.; Ou, J.; Zhang, J.; Lan, W.; Guan, W.; Wu, X.; Yan, Y.; Zhao, W.; Wu, J.; Chodosh, J.; Zhang, Q. COVID-19: Coronavirus Vaccine Development Updates. *Front Immunol* **2020**, *11*, 602256.
5. Liu, W.; Zhou, P.; Chen, K.; Ye, Z.; Liu, F.; Li, X.; He, N.; Wu, Z.; Zhang, Q.; Gong, X.; Tang, Q.; Du, X.; Ying, Y.; Xu, X.; Zhang, Y.; Liu, J.; Li, Y.; Shen, N.; Couban, R.J.; Ibrahim, Q.I.; Guyatt, G.; Zhai, S. Efficacy and safety of antiviral treatment for COVID-19 from evidence in studies of SARS-CoV-2 and other acute viral infections: a systematic review and meta-analysis. *CMAJ* **2020**, *192*, E734–E744.
6. Valle, C.; Martin, B.; Touret, F.; Shannon, A.; Canard, B.; Guillemot, J.C.; Coutard, B.; Decroly, E. Drugs against SARS-CoV-2: What do we know about their mode of action? *Rev Med Virol* **2020**, *30*, 1–10.
7. Grein, J.; Ohmagari, N.; Shin, D.; Diaz, G.; Asperges, E.; Castagna, A.; Feldt, T.; Green, G.; Green, M.L.; Lescure, F.X.; Nicastri, E.; Oda, R.; Yo, K.; Quiros-Roldan, E.; Studemeister, A.; Redinski, J.; Ahmed, S.; Bernett, J.; Chelliah, D.; Chen, D.; Chihara, S.; Cohen, S.H.; Cunningham, J.; D'Arminio Monforte, A.; Ismail, S.; Kato, H.; Lapadula, G.; L'Her, E.; Maeno, T.; Majumder, S.; Massari, M.; Mora-Rillo, M.; Mutoh, Y.; Nguyen, D.; Verweij, E.; Zoufaly, A.; Osinusi, A.O.; DeZure, A.; Zhao, Y.; Zhong, L.; Chokkalingam, A.; Elboudwarej, E.; Telep, L.; Timbs, L.; Henne, I.; Sellers, S.; Cao, H.; Tan, S.K.; Winterbourne, L.; Desai, P.; Mera, R.; Gaggar, A.; Myers, R.P.; Brainard, D.M.; Childs, R.; Flanigan, T. Compassionate Use of Remdesivir for Patients with Severe Covid-19. *N Engl J Med* **2020**, *382*, 2327–2336.
8. Tregoning, J.S.; Brown, E.S.; Cheeseman, H.M.; Flight, K.E.; Higham, S.L.; Lemm, N.M.; Pierce, B.F.; Stirling, D.C.; Wang, Z.; Pollock, K.M. Vaccines for COVID-19. *Clin Exp Immunol* **2020**, *202*, 162–192.
9. European Centre for Disease Prevention and Control. Risk related to spread of new SARS-CoV-2 variants of concern in the EU/EEA, first update. Technical report, Stockholm, 2021.
10. Centers for Disease Control and Prevention (US). SARS-CoV-2 Variants of Concern, 2021.
11. Cui, J.; Li, F.; Shi, Z.L. Origin and evolution of pathogenic coronaviruses. *Nat Rev Microbiol* **2019**, *17*, 181–192.
12. Bar-On, Y.M.; Flamholz, A.; Phillips, R.; Milo, R. Sars-cov-2 (Covid-19) by the numbers. *eLife* **2020**, *9*. doi:10.7554/eLife.57309.

13. Klein, S.; Cortese, M.; Winter, S.L.; Wachsmuth-Melm, M.; Neufeldt, C.J.; Cerikan, B.; Stanifer, M.L.; Boulant, S.; Bartenschlager, R.; Chlanda, P. SARS-CoV-2 structure and replication characterized by *in situ* cryo-electron tomography. *Nature Communications* **2020**, *11*, 1–10. doi:10.1038/s41467-020-19619-7.
14. Turoňová, B.; Sikora, M.; Schürmann, C.; Hagen, W.J.; Welsch, S.; Blanc, F.E.; von Bülow, S.; Gecht, M.; Bagola, K.; Hörner, C.; van Zandbergen, G.; Landry, J.; de Azevedo, N.T.D.; Mosalaganti, S.; Schwarz, A.; Covino, R.; Mühlebach, M.D.; Hummer, G.; Locker, J.K.; Beck, M. *In situ* structural analysis of SARS-CoV-2 spike reveals flexibility mediated by three hinges. *Science* **2020**, *370*, 203–208. doi:10.1126/science.abd5223.
15. Lenard, J. Viral membranes. *Encyclopedia of Virology* **2008**, pp. 308–314. doi:10.1016/B978-012374410-4.00530-6.
16. de Armas-Rillo, L.; Valera, M.S.; Marrero-Hernández, S.; Valenzuela-Fernández, A. Membrane dynamics associated with viral infection. *Reviews in Medical Virology* **2016**, *26*, 146–160, [https://onlinelibrary.wiley.com/doi/pdf/10.1002/rmv.1872]. doi:10.1002/rmv.1872.
17. Miller, S.; Krijnse-Locker, J. Modification of intracellular membrane structures for virus replication. *Nat Rev Microbiol* **2008**, *6*, 363–374. doi:10.1038/nrmicro1890.
18. Ketter, E.; Randall, G. Virus Impact on Lipids and Membranes. *Annual Review of Virology* **2019**, *6*, 319–340. PMID: 31567065, doi:10.1146/annurev-virology-092818-015748.
19. Schweizer, A.; Clausen, H.; Van Meer, G.; Hauri, H.P. Localization of O-glycan initiation, sphingomyelin synthesis, and glucosylceramide synthesis in Vero cells with respect to the endoplasmic reticulum-Golgi intermediate compartment. *Journal of Biological Chemistry* **1994**, *269*, 4035–4041. doi:10.1016/s0021-9258(17)41738-8.
20. Mandala, V.S.; McKay, M.J.; Shcherbakov, A.A.; Dregni, A.J.; Kolocouris, A.; Hong, M. Structure and drug binding of the SARS-CoV-2 envelope protein transmembrane domain in lipid bilayers. *Nature Structural and Molecular Biology* **2020**, *27*, 1202–1208. doi:10.1038/s41594-020-00536-8.
21. Renz, A.; Widerspick, L.; Dräger, A. FBA reveals guanylate kinase as a potential target for antiviral therapies against SARS-CoV-2. *Bioinformatics* **2020**, *36*, i813–i821. doi:10.1093/bioinformatics/btaa813.
22. Bordbar, A.; Lewis, N.E.; Schellenberger, J.; Palsson, B.; Jamshidi, N. Insight into human alveolar macrophage and *M. tuberculosis* interactions via metabolic reconstructions. *Molecular Systems Biology* **2010**, *6*. doi:10.1038/msb.2010.68.
23. Hible, G.; Daalova, P.; Gilles, A.M.; Cherfils, J. Crystal structures of GMP kinase in complex with ganciclovir monophosphate and Ap5G. *Biochimie* **2006**, *88*, 1157–1164.
24. Navé, J.F.; Eschbach, A.; Halazy, S. 9-(Phosphonoalkyl)guanine derivatives as substrates or inhibitors of guanylate kinase. *Archives of Biochemistry and Biophysics* **1992**, *295*, 253–257. doi:10.1016/0003-9861(92)90515-X.
25. Navé, J.F.; Taylor, D.; Tyms, S.; Kenny, M.; Eggenspiller, A.; Eschbach, A.; Dulworth, J.; Brennan, T.; Piriou, F.; Halazy, S. Synthesis, antiviral activity and enzymatic phosphorylation of 9-phosphonopentenyl derivatives of guanine. *Antiviral Research* **1995**, *27*, 301–316. doi:10.1016/0166-3542(95)00023-F.
26. Aller, S.; Scott, A.; Sarkar-Tyson, M.; Soyer, O.S. Integrated human-virus metabolic stoichiometric modelling predicts host-based antiviral targets against Chikungunya, Dengue and Zika viruses. *Journal of the Royal Society Interface* **2018**, *15*. doi:10.1098/rsif.2018.0125.
27. Tilocca, B.; Soggiu, A.; Sanguinetti, M.; Babini, G.; De Maio, F.; Britti, D.; Zecconi, A.; Bonizzi, L.; Urbani, A.; Roncada, P. Immunoinformatic analysis of the SARS-CoV-2 envelope protein as a strategy to assess cross-protection against COVID-19. *Microbes and Infection* **2020**, *22*, 182–187. doi:10.1016/j.micinf.2020.05.013.
28. Stodola, J.K.; Dubois, G.; Le Coupanec, A.; Desforges, M.; Talbot, P.J. The OC43 human coronavirus envelope protein is critical for infectious virus production and propagation in neuronal cells and is a determinant of neurovirulence and CNS pathology. *Virology* **2018**, *515*, 134–149. doi:10.1016/j.virol.2017.12.023.
29. Godet, M.; L'Haridon, R.; Vautherot, J.F.; Laude, H. TGEV corona virus ORF4 encodes a membrane protein that is incorporated into virions. *Virology* **1992**, *188*, 666–675. doi:10.1016/0042-6822(92)90521-P.
30. Yao, H.; Song, Y.; Chen, Y.; Wu, N.; Xu, J.; Sun, C.; Zhang, J.; Weng, T.; Zhang, Z.; Wu, Z.; Cheng, L.; Shi, D.; Lu, X.; Lei, J.; Crispin, M.; Shi, Y.; Li, L.; Li, S. Molecular Architecture of the SARS-CoV-2 Virus. *Cell* **2020**, *183*, 730–738.e13. doi:10.1016/j.cell.2020.09.018.
31. Lu, S.; Ye, Q.; Singh, D.; Cao, Y.; Diedrich, J.K.; Yates, J.R.; Villa, E.; Cleveland, D.W.; Corbett, K.D. The SARS-CoV-2 nucleocapsid phosphoprotein forms mutually exclusive condensates with RNA and the membrane-associated M protein. *Nature Communications* **2021**, *12*, 1–15. doi:10.1038/s41467-020-20768-y.
32. Neuman, B.W.; Kiss, G.; Kunding, A.H.; Bhella, D.; Baksh, M.F.; Connelly, S.; Droese, B.; Klaus, J.P.; Makino, S.; Sawicki, S.G.; Siddell, S.G.; Stamou, D.G.; Wilson, I.A.; Kuhn, P.; Buchmeier, M.J. A structural analysis of M protein in coronavirus assembly and morphology. *Journal of Structural Biology* **2011**, *174*, 11–22. doi:10.1016/j.jsb.2010.11.021.
33. Pedley, A.M.; Benkovic, S.J. A New View into the Regulation of Purine Metabolism: The Purinosome. *Trends in Biochemical Sciences* **2017**, *42*, 141–154. doi:10.1016/j.tibs.2016.09.009.
34. Löffler, M.; Fairbanks, L.D.; Zameitat, E.; Marinaki, A.M.; Simmonds, H.A. Pyrimidine pathways in health and disease. *Trends in Molecular Medicine* **2005**, *11*, 430–437. doi:10.1016/j.molmed.2005.07.003.
35. Norsigian, C.J.; Pusarla, N.; McConn, J.L.; Yurkovich, J.T.; Dräger, A.; Palsson, B.O.; King, Z. BiGG Models 2020: multi-strain genome-scale models and expansion across the phylogenetic tree. *Nucleic Acids Research* **2019**. doi:10.1093/nar/gkz1054.
36. Elbe, S.; Buckland-Merrett, G. Data, disease and diplomacy: GISAID's innovative contribution to global health. *Global Challenges* **2017**, *1*, 33–46. doi:10.1002/gch2.1018.

37. Shu, Y.; McCauley, J. GISAID: Global initiative on sharing all influenza data – from vision to reality. *Eurosurveillance* **2017**, *22*, 30494. doi:10.2807/1560-7917.ES.2017.22.13.30494.
38. Abassi, Z.; Knaney, Y.; Karram, T.; Heyman, S.N. The Lung Macrophage in SARS-CoV-2 Infection: A Friend or a Foe? *Frontiers in Immunology* **2020**, *11*, 1312. doi:10.3389/fimmu.2020.01312.
39. Qi, F.; Qian, S.; Zhang, S.; Zhang, Z. Single cell RNA sequencing of 13 human tissues identify cell types and receptors of human coronaviruses. *Biochemical and Biophysical Research Communications* **2020**, *526*, 135–140. doi:10.1016/j.bbrc.2020.03.044.
40. Joel Funk, C.; Wang, J.; Ito, Y.; Travanty, E.A.; Voelker, D.R.; Holmes, K.V.; Mason, R.J. Infection of human alveolar macrophages by human coronavirus strain 229E. *Journal of General Virology* **2012**, *93*, 494–503. doi:10.1099/vir.0.038414-0.
41. Al-Qahtani, A.A.; Lyroni, K.; Aznaourova, M.; Tseliou, M.; Al-Anazi, M.R.; Al-Ahdal, M.N.; Alkahtani, S.; Sourvinos, G.; Tsatsanis, C. Middle east respiratory syndrome corona virus spike glycoprotein suppresses macrophage responses via DPP4-mediated induction of IRAK-M and PPARγ. *Oncotarget* **2017**, *8*, 9053–9066. doi:10.18632/oncotarget.14754.
42. Gu, J.; Gong, E.; Zhang, B.; Zheng, J.; Gao, Z.; Zhong, Y.; Zou, W.; Zhan, J.; Wang, S.; Xie, Z.; Zhuang, H.; Wu, B.; Zhong, H.; Shao, H.; Fang, W.; Gao, D.; Pei, F.; Li, X.; He, Z.; Xu, D.; Shi, X.; Anderson, V.M.; Leong, A.S. Multiple organ infection and the pathogenesis of SARS. *Journal of Experimental Medicine* **2005**, *202*, 415–424. doi:10.1084/jem.20050828.
43. Chu, H.; Chan, J.F.W.; Wang, Y.; Yuen, T.T.T.; Chai, Y.; Hou, Y.; Shuai, H.; Yang, D.; Hu, B.; Huang, X.; Zhang, X.; Cai, J.P.; Zhou, J.; Yuan, S.; Kok, K.H.; To, K.K.W.; Chan, I.H.Y.; Zhang, A.J.; Sit, K.Y.; Au, W.K.; Yuen, K.Y. Comparative Replication and Immune Activation Profiles of SARS-CoV-2 and SARS-CoV in Human Lungs: An Ex Vivo Study With Implications for the Pathogenesis of COVID-19. *Clinical Infectious Diseases* **2020**, *71*, 1400–1409, [https://academic.oup.com/cid/article-pdf/71/6/1400/33738683/ciaa410.pdf]. doi:10.1093/cid/ciaa410.
44. Dalskov, L.; Møhlenberg, M.; Thyrsted, J.; Blay-Cadanet, J.; Poulsen, E.T.; Folkersen, B.H.; Skaarup, S.H.; Olagnier, D.; Reinert, L.; Enghild, J.J.; Hoffmann, H.J.; Holm, C.K.; Hartmann, R. SARS-CoV-2 evades immune detection in alveolar macrophages. *EMBO reports* **2020**, *21*, e51252, [https://www.embopress.org/doi/pdf/10.15252/embr.202051252]. doi:10.15252/embr.202051252.
45. Delattre, H.; Sasidharan, K.; Soyer, O.S. Inhibiting the reproduction of SARS-CoV-2 through perturbations in human lung cell metabolic network. *Life Science Alliance* **2021**, *4*. doi:10.26508/LSA.202000869.
46. Swainston, N.; Smallbone, K.; Hefzi, H.; Dobson, P.D.; Brewer, J.; Hanscho, M.; Zielinski, D.C.; Ang, K.S.; Gardiner, N.J.; Gutierrez, J.M.; Kyriakopoulos, S.; Lakshmanan, M.; Li, S.; Liu, J.K.; Martínez, V.S.; Orellana, C.A.; Quek, L.E.; Thomas, A.; Zanghellini, J.; Borth, N.; Lee, D.Y.; Nielsen, L.K.; Kell, D.B.; Lewis, N.E.; Mendes, P. Recon 2.2: from reconstruction to model of human metabolism. *Metabolomics* **2016**, *12*, 109. doi:10.1007/s11306-016-1051-4.
47. Rahman, M.R.; Banik, A.; Chowdhury, I.M.; Sajib, E.H.; Sarkar, S. Identification of potential antivirals against SARS-CoV-2 using virtual screening method. *Informatics in Medicine Unlocked* **2021**, *23*, 100531. doi:10.1016/j.imu.2021.100531.
48. Hussien, M.A.; Abdelaziz, A.E. Molecular docking suggests repurposing of brincidofovir as a potential drug targeting SARS-CoV-2 ACE2 receptor and main protease. *Network Modeling Analysis in Health Informatics and Bioinformatics* **2020**, *9*, 1–18. doi:10.1007/s13721-020-00263-6.
49. National Library of Medicine (U.S.). ClinicalTrials.gov, 2020.
50. Bojkova, D.; Costa, R.; Bechtel, M.; Ciesek, S.; Michaelis, M.; Cinatl, J. Targeting pentose phosphate pathway for SARS-CoV-2 therapy. *bioRxiv* **2020**, p. 2020.08.19.257022. doi:10.1101/2020.08.19.257022.
51. Zhang, Y.; Guo, R.; Kim, S.H.; Shah, H.; Zhang, S.; Liang, J.H.; Fang, Y.; Gentili, M.; Leary, C.N.; Elledge, S.J.; Hung, D.T.; Mootha, V.K.; Gewurz, B.E. SARS-CoV-2 hijacks folate and one-carbon metabolism for viral replication. *Nature Communications* **2021**, *12*, 1–11. doi:10.1038/s41467-021-21903-z.
52. Caruso, A.; Caccuri, F.; Bugatti, A.; Zani, A.; Vanoni, M.; Bonfanti, P.; Cazzaniga, M.E.; Perno, C.F.; Messa, C.; Alberghina, L. Methotrexate inhibits SARS-CoV-2 virus replication "in vitro". *Journal of Medical Virology* **2021**, *93*, 1780–1785. doi:10.1002/jmv.26512.
53. Stegmann, K.M.; Dickmanns, A.; Gerber, S.; Nikolova, V.; Klemke, L.; Manzini, V.; Schlösser, D.; Bierwirth, C.; Freund, J.; Sitte, M.; Lugert, R.; Salinas, G.; Görlich, D.; Wollnik, B.; Groß, U.; Dobbelstein, M. The folate antagonist methotrexate diminishes replication of the coronavirus SARS-CoV-2 and enhances the antiviral efficacy of remdesivir in cell culture models. *bioRxiv* **2020**, p. 2020.07.18.210013. doi:10.1101/2020.07.18.210013.
54. Coelho, A.R.; Oliveira, P.J. Dihydroorotate dehydrogenase inhibitors in SARS-CoV-2 infection. *European Journal of Clinical Investigation* **2020**, *50*, e13366. doi:10.1111/eci.13366.
55. Hoffmann, H.H.; Kunz, A.; Simon, V.A.; Palese, P.; Shaw, M.L. Broad-spectrum antiviral that interferes with *de novo* pyrimidine biosynthesis. *Proceedings of the National Academy of Sciences of the United States of America* **2011**, *108*, 5777–5782. doi:10.1073/pnas.1101143108.
56. Cheung, N.N.; Lai, K.K.; Dai, J.; Kok, K.H.; Chen, H.; Chan, K.H.; Yuen, K.Y.; Tsun Kao, R.Y. Broad-spectrum inhibition of common respiratory RNA viruses by a pyrimidine synthesis inhibitor with involvement of the host antiviral response. *Journal of General Virology* **2017**, *98*, 946–954. doi:10.1099/jgv.0.000758.
57. Chen, S.; Ding, S.; Yin, Y.; Xu, L.; Li, P.; Peppelenbosch, M.P.; Pan, Q.; Wang, W. Suppression of pyrimidine biosynthesis by targeting DHODH enzyme robustly inhibits rotavirus replication. *Antiviral Research* **2019**, *167*, 35–44. doi:10.1016/j.antiviral.2019.04.005.
58. Luthra, P.; Naidoo, J.; Pietzsch, C.A.; De, S.; Khadka, S.; Anantpadma, M.; Williams, C.G.; Edwards, M.R.; Davey, R.A.; Bukreyev, A.; Ready, J.M.; Basler, C.F. Inhibiting pyrimidine biosynthesis impairs Ebola virus replication through depletion of nucleoside pools and activation of innate immune responses. *Antiviral Research* **2018**, *158*, 288–302. doi:10.1016/j.antiviral.2018.08.012.

59. Luban, J.; Sattler, R.A.; Mühlberger, E.; Graci, J.D.; Cao, L.; Weetall, M.; Trotta, C.; Colacino, J.M.; Bavari, S.; Strambio-De-Castillia, C.; Suder, E.L.; Wang, Y.; Soloveva, V.; Cintron-Lue, K.; Naryshkin, N.A.; Pykett, M.; Welch, E.M.; O'Keefe, K.; Kong, R.; Goodwin, E.; Jacobson, A.; Paessler, S.; Peltz, S.W. The DHODH inhibitor PTC299 arrests SARS-CoV-2 replication and suppresses induction of inflammatory cytokines. *Virus Research* **2021**, *292*, 198246. doi:10.1016/j.virusres.2020.198246.
60. Xiong, R.; Zhang, L.; Li, S.; Sun, Y.; Ding, M.; Wang, Y.; Zhao, Y.; Wu, Y.; Shang, W.; Jiang, X.; Shan, J.; Shen, Z.; Tong, Y.; Xu, L.; Chen, Y.; Liu, Y.; Zou, G.; Lavillette, D.; Zhao, Z.; Wang, R.; Zhu, L.; Xiao, G.; Lan, K.; Li, H.; Xu, K. Novel and potent inhibitors targeting DHODH are broad-spectrum antivirals against RNA viruses including newly-emerged coronavirus SARS-CoV-2. *Protein and Cell* **2020**, *11*, 723–739. doi:10.1007/s13238-020-00768-w.
61. Grant, O.C.; Montgomery, D.; Ito, K.; Woods, R.J. Analysis of the SARS-CoV-2 spike protein glycan shield reveals implications for immune recognition. *Scientific Reports* **2020**, *10*, 1–11. doi:10.1038/s41598-020-71748-7.
62. Watanabe, Y.; Allen, J.D.; Wrapp, D.; McLellan, J.S.; Crispin, M. Site-specific glycan analysis of the SARS-CoV-2 spike. *Science* **2020**, *369*, 330–333. doi:10.1126/science.abb9983.
63. Abu-Farha, M.; Thanaraj, T.A.; Qaddoumi, M.G.; Hashem, A.; Abubaker, J.; Al-Mulla, F. The Role of Lipid Metabolism in COVID-19 Virus Infection and as a Drug Target. *International Journal of Molecular Sciences* **2020**, *21*, 3544. doi:10.3390/ijms21103544.
64. Wu, Q.; Zhou, L.; Sun, X.; Yan, Z.; Hu, C.; Wu, J.; Xu, L.; Li, X.; Liu, H.; Yin, P.; Li, K.; Zhao, J.; Li, Y.; Wang, X.; Li, Y.; Zhang, Q.; Xu, G.; Chen, H. Altered Lipid Metabolism in Recovered SARS Patients Twelve Years after Infection. *Scientific Reports* **2017**, *7*, 1–12. doi:10.1038/s41598-017-09536-z.
65. Nguyen, A.; Guedán, A.; Mousnier, A.; Swieboda, D.; Zhang, Q.; Horkai, D.; Le Novere, N.; Solari, R.; Wakelam, M.J. Host lipidome analysis during rhinovirus replication in HBECs identifies potential therapeutic target. *Journal of Lipid Research* **2018**, *59*, 1671–1684. doi:10.1194/jlr.M085910.
66. Yan, B.; Zou, Z.; Chu, H.; Chan, G.; Tsang, J.O.L.; Lai, P.M.; Yuan, S.; Yip, C.C.Y.; Yin, F.; Kao, R.Y.T.; Sze, K.H.; Lau, S.K.P.; Chan, J.F.W.; Yuen, K.Y. Lipidomic Profiling Reveals Significant Perturbations of Intracellular Lipid Homeostasis in Enterovirus-Infected Cells. *International Journal of Molecular Sciences* **2019**, *20*, 5952. doi:10.3390/ijms20235952.
67. Yan, B.; Chu, H.; Yang, D.; Sze, K.H.; Lai, P.M.; Yuan, S.; Shuai, H.; Wang, Y.; Kao, R.Y.T.; Chan, J.F.W.; Yuen, K.Y. Characterization of the lipidomic profile of human coronavirus-infected cells: Implications for lipid metabolism remodeling upon coronavirus replication. *Viruses* **2019**, *11*. doi:10.3390/v11010073.
68. Visioli, F.; Colombo, C.; Monti, S.; Giulidori, P.; Galli, C. S-adenosyl-L-methionine: Role in phosphatidylcholine synthesis and in vitro effects on the ethanol-induced alterations of lipid metabolism. *Pharmacological Research* **1998**, *37*, 203–206. doi:10.1006/phrs.1997.0282.
69. Ye, C.; Sutter, B.M.; Wang, Y.; Kuang, Z.; Tu, B.P. A Metabolic Function for Phospholipid and Histone Methylation. *Molecular Cell* **2017**, *66*, 180–193.e8. doi:10.1016/j.molcel.2017.02.026.
70. Malik-Sheriff, R.S.; Glont, M.; Nguyen, T.V.N.; Tiwari, K.; Roberts, M.G.; Xavier, A.; Vu, M.T.; Men, J.; Maire, M.; Kananathan, S.; Fairbanks, E.L.; Meyer, J.P.; Arankalle, C.; Varusai, T.M.; Knight-Schrijver, V.; Li, L.; Dueñas-Roca, C.; Dass, G.; Keating, S.M.; Park, Y.M.; Buso, N.; Rodriguez, N.; Hucka, M.; Hermjakob, H. BioModels—15 years of sharing computational models in life science. *Nucleic Acids Research* **2020**, *48*, D407–D415. doi:10.1093/nar/gkz1055.
71. Keating, S.M.; Waltemath, D.; König, M.; Zhang, F.; Dräger, A.; Chaouiya, C.; Bergmann, F.T.; Finney, A.; Gillespie, C.S.; Helikar, T.; Hoops, S.; Malik-Sheriff, R.S.; Moodie, S.L.; Moraru, I.I.; Myers, C.J.; Naldi, A.; Olivier, B.G.; Sahle, S.; Schaff, J.C.; Smith, L.P.; Swat, M.J.; Thieffry, D.; Watanabe, L.; Wilkinson, D.J.; Blinov, M.L.; Begley, K.; Faeder, J.R.; Gómez, H.F.; Hamm, T.M.; Inagaki, Y.; Liebermeister, W.; Lister, A.L.; Lucio, D.; Mjolsness, E.; Proctor, C.J.; Raman, K.; Rodriguez, N.; Shaffer, C.A.; Shapiro, B.E.; Stelling, J.; Swainston, N.; Tanimura, N.; Wagner, J.; Meier-Schellersheim, M.; Sauro, H.M.; Palsson, B.; Bolouri, H.; Kitano, H.; Funahashi, A.; Hermjakob, H.; Doyle, J.C.; Hucka, M.; Adams, R.R.; Allen, N.A.; Angermann, B.R.; Antoniotti, M.; Bader, G.D.; Červený, J.; Courtot, M.; Cox, C.D.; Dalle Pezze, P.; Demir, E.; Denney, W.S.; Dharuri, H.; Dorier, J.; Drasdo, D.; Ebrahim, A.; Eichner, J.; Elf, J.; Endler, L.; Evelo, C.T.; Flamm, C.; Fleming, R.M.T.; Fröhlich, M.; Glont, M.; Gonçalves, E.; Golebiewski, M.; Grabski, H.; Gutteridge, A.; Hachmeister, D.; Harris, L.A.; Heavner, B.D.; Henkel, R.; Hlavacek, W.S.; Hu, B.; Hyduke, D.R.; Jong, H.; Juty, N.; Karp, P.D.; Karr, J.R.; Kell, D.B.; Keller, R.; Kiselev, I.; Klamt, S.; Klipp, E.; Knüpfer, C.; Kolpakov, F.; Krause, F.; Kutmon, M.; Laibe, C.; Lawless, C.; Li, L.; Loew, L.M.; Machne, R.; Matsuoka, Y.; Mendes, P.; Mi, H.; Mittag, F.; Monteiro, P.T.; Natarajan, K.N.; Nielsen, P.M.F.; Nguyen, T.; Palmisano, A.; Pettit, J.; Pfau, T.; Phair, R.D.; Radivoyevitch, T.; Rohwer, J.M.; Ruebenacker, O.A.; Saez-Rodriguez, J.; Scharm, M.; Schmidt, H.; Schreiber, F.; Schubert, M.; Schulte, R.; Sealfon, S.C.; Smallbone, K.; Soliman, S.; Stefan, M.I.; Sullivan, D.P.; Takahashi, K.; Teusink, B.; Tolnay, D.; Vazirabad, I.; Kamp, A.v.; Wittig, U.; Wrzodek, C.; Wrzodek, F.; Xenarios, I.; Zhukova, A.; Zucker, J. SBML Level 3: an extensible format for the exchange and reuse of biological models. *Molecular Systems Biology* **2020**, *16*, e9110, [https://www.embopress.org/doi/pdf/10.15252/msb.20199110]. doi:10.15252/msb.20199110.
72. Renz, A.; Mostolizadeh, R.; Dräger, A. Clinical Applications of Metabolic Models in SBML Format. In *Systems Medicine*; Wolkenhauer, O., Ed.; Academic Press: Oxford, 2020; Vol. 3, pp. 362–371. doi:10.1016/B978-0-12-801238-3.11524-7.
73. Hucka, M.; Bergmann, F.T.; Dräger, A.; Hoops, S.; Keating, S.M.; Le Novère, N.; Myers, C.J.; Olivier, B.G.; Sahle, S.; Schaff, J.C.; Smith, L.P.; Waltemath, D.; Wilkinson, D.J. Systems Biology Markup Language (SBML) Level 3 Version 1 Core. *Journal of Integrative Bioinformatics* **2018**, *15*, 1. doi:10.1515/jib-2017-0080.
74. Olivier, B.G.; Bergmann, F.T. SBML Level 3 Package: Flux Balance Constraints version 2. *Journal of Integrative Bioinformatics* **2018**, *15*. doi:10.1515/jib-2017-0082.

75. Bergmann, F.T.; Adams, R.; Moodie, S.; Cooper, J.; Glont, M.; Golebiewski, M.; Hucka, M.; Laibe, C.; Miller, A.K.; Nickerson, D.P.; Olivier, B.G.; Rodriguez, N.; Sauro, H.M.; Scharm, M.; Soiland-Reyes, S.; Waltemath, D.; Yvon, F.; Le Novère, N. COMBINE archive and OMEX format: one file to share all information to reproduce a modeling project. *BMC Bioinformatics* **2014**, *15*, 369. doi:10.1186/s12859-014-0369-z.

Table A1. Reactions from the host-derived enforcement experiments. The reaction identifiers listed in figure 1 on page 4 are BIGG identifier [35]. In this table, the BIGG reaction identifiers are given, together with the reaction name and the subsystem, they occur in.

Reaction-ID	Reaction name	Subsystem
ADSL1	Adenylosuccinate lyase 1	Purine metabolism
ADSL2	Adenylosuccinate lyase 2	Purine metabolism
ADSS	Adenylosuccinate synthase	Purine metabolism
AICART	Phosphoribosylaminoimidazolecarboxamide formyltransferase	Purine metabolism
AIRCr	Phosphoribosylaminoimidazole carboxylase	Purine metabolism
ASPCTr	Aspartate carbamoyltransferase	Pyrimidine metabolism
CBPS	Carbamoyl-phosphate synthase	Pyrimidine metabolism
DHORD9	Dihydoorotic acid dehydrogenase	Pyrimidine metabolism
DHORTS	Dihydroorotase	Pyrimidine metabolism
GARFT	Phosphoribosylglycinamide formyltransferase	Purine metabolism
GK1	Guanylate kinase	Purine metabolism
GLUPRT	Glutamine phosphoribosyldiphosphate amidotransferase	Purine metabolism
IMPC	IMP cyclohydrolase	Purine metabolism
OMPDC	Orotidine-5′-phosphate decarboxylase	Pyrimidine metabolism
ORPT	Orotate phosphoribosyltransferase	Pyrimidine metabolism
PRAGSr	Phosphoribosylglycinamide synthase	Purine metabolism
PRAIS	Phosphoribosylaminoimidazole synthase	Purine metabolism
PRASCS	Phosphoribosylaminoimidazolesuccinocarboxamide synthase	Purine metabolism
PRFGS	Phosphoribosylformylglycinamidine synthase	Purine metabolism
PRPPS	Phosphoribosylpyrophosphate synthetase	Pentose phosphate pathway
RPI	Ribose-5-phosphate isomerase	Pentose phosphate pathway